International Journal of Safety and Security Engineering
Vol. 16, No. 2, February, 2026, pp. 263-274
Journal homepage: http://iieta.org/journals/ijsse

Application of Geoelectrical Methods for Mapping Unstable Areas in the Guarumales Camp-Ecuador

Edgar Molina-Torres[1], Roberto Avalos-Sánchez[1], Jessica Robles[2], Joselyne Solórzano[1,3*], Paúl Carrión-Mero[1,3]

[1] Facultad de Ingeniería en Ciencias de la Tierra, ESPOL Polytechnic University, ESPOL, Guayaquil 090902, Ecuador
[2] CELEC Sur Business Unit, Corporación Eléctrica del Ecuador (CELEC EP), Cuenca 010603, Ecuador
[3] Centro de Investigación y Proyectos Aplicados a las Ciencias de la Tierra, ESPOL Polytechnic University, ESPOL, Guayaquil 090902, Ecuador

Corresponding Author Email: josbasol@espol.edu.ec

https://doi.org/10.18280/ijsse.160202

Received: 12 December 2025
Revised: 3 February 2026
Accepted: 17 February 2026
Available online: 28 February 2026

Keywords:
electrical resistivity tomography, vertical electrical soundings, landslide, slope stability, susceptibility analysis, mapping

ABSTRACT

Mass movements are geological processes involving the downslope displacement of soil and rock, often resulting in significant economic losses and threats to human safety. The presence of large hydroelectric infrastructures may further increase the susceptibility of surrounding slopes to instability. The Paute Integral Project in Azuay, Ecuador, comprises three major dams that supply approximately 30% of the country's electricity demand. The Guarumales camp is located within an active translational macro-landslide characterized by two internal failure planes and the presence of an aquifer that strongly influences slope dynamics. This study aims to produce a landslide susceptibility map for the Guarumales camp through the integration of geophysical techniques and spatial analysis. Electrical Resistivity Tomography (ERT) and Vertical Electrical Soundings (VES) were applied to characterize subsurface conditions and identify zones of potential instability. The methodological framework consisted of four main stages: (i) Characterization of instability factors using baseline thematic data, (ii) geophysical survey and data acquisition, (iii) spatial analysis and mapping using Geographic Information System (GIS), and (iv) generation of a landslide susceptibility map. The integrated analysis revealed that areas with low resistivity values (<75 Ω·m), weak geological materials, and high water saturation on steep slopes correspond to zones of high instability. Additional instability was identified along stream banks due to erosion and undercutting processes, as well as in groundwater recharge areas. Conversely, zones characterized by high resistivity values (>7,000 Ω·m) and dense forest cover exhibited relatively greater slope stability. The resulting susceptibility zonation provides valuable information for land-use planning and the development of mitigation strategies based on field evaluations. These findings contribute to improving risk management in hydroelectric projects located in geologically complex and landslide-prone environments.

1. INTRODUCTION

Mass movements are among the most destructive natural hazards, causing significant damage to infrastructure and posing a serious threat to human life [1]. These natural processes, characterized by the downslope displacement of soil and rock masses, are common in regions where topographic, geological, meteorological, and hydrogeological conditions interact to create inherently unstable environments [2]. These unstable conditions often coincide with areas developed for hydropower generation due to their high hydraulic potential [3]. Hydropower plants are commonly located in mountainous, steep-slope regions prone to landslides, where materials with low geomechanical strength, residual soils, fractured rock masses, and intense precipitation are common [4].

Currently, Ecuador has 15 hydropower plants, accounting for 72.79% of the country's total installed generation capacity [5], with an effective installed capacity of 6,855.07 MW [6].

Among the eight business units of the Corporación Eléctrica del Ecuador (CELEC EP) that operate hydropower facilities, CELEC SUR stands out as the unit with the highest hydropower production capacity nationwide, reaching 2,027 Megawatts (MW). Of this output, about 87% corresponds to the Paute Integral Hydropower Complex (PIHC), which comprises the Mazar, Paute-Molino, and Sopladora projects [5].

The hydropower project is in Azuay Province, along the Paute–Guarumales–Méndez roadway, which is part of the E-40 highway (Figure 1).

In 2020, CELEC EP recorded twenty-one mass movements, including the Guarumales landslide in the camp associated with the operation of the Paute–Molino Hydropower Plant [7].

In the areas surrounding the PIHC, landslides have been

identified that have damaged road infrastructure, resulting in accessibility issues to the complex's central operational facility the Guarumales camp. In this area, landslides have occurred that have completely disrupted the roadway; a representative example took place in June 2020 at the Jurupis stream (Amaluza Parish), where an approximately 80 m section of the road failed, necessitating a realignment of the roadway axis and the construction of a new bridge [8].

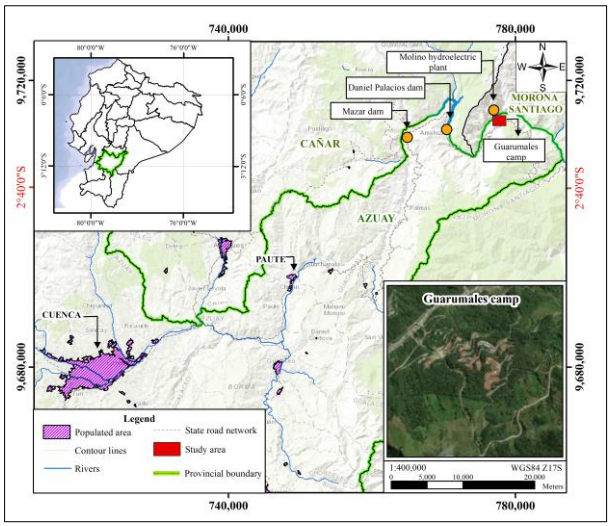

Figure 1. Location map of the Paute Integral Hydropower Complex (PIHC) in the Azuay province and the Guarumales camp

The assessment of the Guarumales landslide led CELEC EP to implement a range of investigation techniques, including geodetic monitoring, the installation of piezometers and rain gauges, flow measurements in drainage systems, and geotechnical borehole campaigns. These investigations determined that the Guarumales landslide is approximately 1.5 km² in area, deep-seated, and exhibits slow-moving behavior with velocities of approximately 50 mm per year [4]. Furthermore, through empirical correlation of geophysical methods—Vertical Electrical Soundings (VES) and H/V spectral ratio analysis— it was established that the landslide corresponds to a translational mechanism associated with thick colluvial deposits exceeding 55 m in thickness. These potentially unstable materials are deposited on metamorphic schists [9]. These deposits are permeable and poorly saturated, where local infiltration processes play a significant role in the landslide's evolution [4].

In this context, developing a landslide susceptibility map is fundamental for identifying areas with the highest probability of instability and anticipating risk scenarios. Electrical Resistivity Tomography (ERT) and VES have been applied in geophysical exploration campaigns to delineate saturated zones, lithological contrasts, and potential landslide rupture surfaces [10-13].

Similarly, several authors emphasize that adequate characterization of abiotic elements—such as lithology, geomorphology, soils, and geodynamic processes—is essential for understanding ground stability and for planning territorial management actions that reduce the risk to hydroelectric infrastructure and nearby populations [14].

Based on this context, the following research questions arise: (i) How can unstable areas be delineated through the application of geophysical methods in the Guarumales camp? and (ii) How does geoelectrical surveying contribute to the development of an instability zoning map that enables the assessment of the geotechnical safety of existing infrastructure?

To strengthen the control measures applied at the camp, this study aims to generate a slope stability zoning map by correlating geophysical methods (ERT and VES) to identify critical areas requiring complementary investigations.

2. MATERIALS AND METHODS

Mass movement zoning methods consider multiple factors to estimate susceptibility to these natural processes. Such approaches integrate semi-quantitative assessments that weight conditioning and triggering factors [15]. Likewise, these analyses incorporate site knowledge criteria by selecting relevant factors, assigning them ranks and weights based on their relative importance [16]. This framework is complemented by surface-based geophysical measurements, including electrical resistivity, to zone by degree of instability and define priority areas for intervention.

The methodological approach was divided into four phases: (1) characterization of instability factors based on baseline thematic information, (2) geophysical exploration campaign, (3) Geographic Information System (GIS)-based mapping, and (4) mapping of unstable areas (Figure 2).

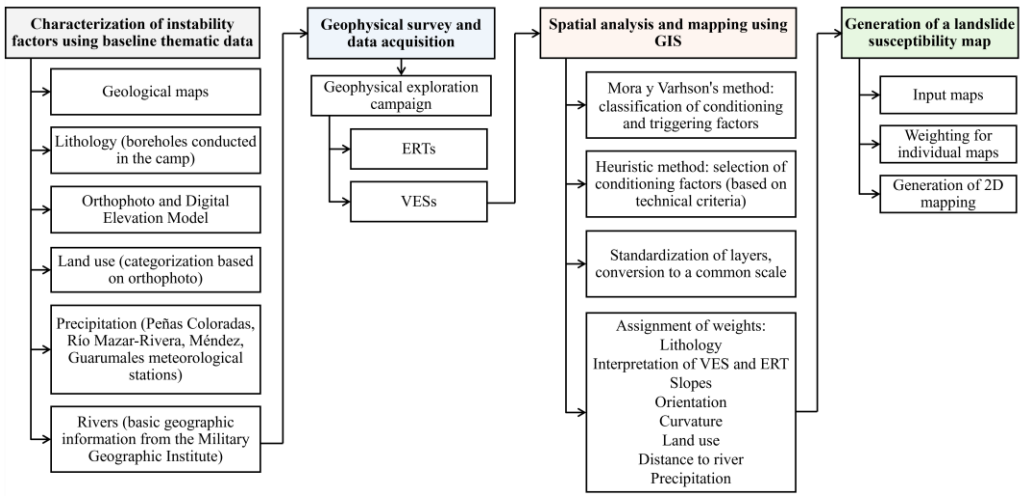

Figure 2. Outline of the methodological process for zoning unstable areas

2.1 Phase I: Characterization of instability factors based on baseline thematic information

Preliminary and essential information for mass movement zoning was analyzed and compiled, including the Cañar and Sucúa geological map sheets at a 1:100,000 scale from the Geological and Energy Research Institute (IIGE, acronym in spanish); the geological map of the Sevilla de Oro canton at a 1:25,000 scale from the Natural Disaster Prevention Project in the Paute Basin (PRECUPA, acronym in spanish); borehole records from the Guarumales camp conducted in November 2016; a Digital Elevation Model (DEM) and 1:5,000-scale orthophotography from the Ministry of Agriculture and Livestock (MAGAP, acronym in spanish); historical data from the Peñas Coloradas, Río Mazar–Rivera, and Méndez meteorological stations of the National Institute of Meteorology and Hydrology of Ecuador (INAMHI, acronym in spanish), data from the meteorological station located within the Guarumales camp operated by the CELEC SUR, geological map, stratigraphic columns and a conceptual model of the macro-landslide [4].

2.2 Phase II: Geophysical exploration campaign

The layout and positioning of the geophysical survey lines were determined through site inspections of areas within the Guarumales camp that showed evidence of instability, including subsidence, undercutting, pavement loss, material detachment, erosion, and failures in retaining structures. During the geophysical exploration campaign, electrical methods (VES and ERT) were applied using an ABEM Terrameter LS-2 system.

The geophysical campaign included eight VESs with investigation depths ranging from 98 to 147 m, using a Schlumberger array, and sixteen ERT profiles with lengths of 200 m and 400 m, achieving investigation depths of approximately 40 m and 80 m, respectively, using a gradient array. This approach enabled the acquisition of one and two-dimensional electrical resistivity profiles, allowing the determination of material thicknesses, the identification of saturated zones, and the interpretation of geological structures.

2.3 Phase III: Geographic Information System-based mapping

Based on information obtained during the initial phases, cartographic inputs for the analysis of unstable area zoning were generated using GIS tools.

The map of lithological units and structural lineaments was generated based on field-identified outcrops, analysis of lithological logs, interpretation of VES and ERT data, and photointerpretation of the DEM and orthophotography obtained from MAGAP.

The electrical resistivity map was developed by correlating VES and ERT survey with the dominant stratigraphic units. A spatial interpolation process using the Inverse Distance Weighted (IDW) method was applied within a GIS environment to uniformly represent surface resistivity values, reflecting the distribution of materials and saturated zones [17].

Based on the DEM, a slope map was generated, with slope intervals defined in degrees using the GIS natural classification method, and aspect angles determined in azimuth degrees ranging from 0° to 360° relative to geographic north [18]. In addition, terrain concavity and convexity were derived with respect to the direction of maximum slope to identify zones of flow concentration and dispersion [19].

A supervised classification was implemented in a GIS environment using spectral signatures derived from orthophotography, following the guidelines of Sharma Banjade et al. [20] to determine land use. Additionally, the drainage network's zones of influence were delineated using the GIS buffer tool, establishing spatial intervals that represent the relationship between fluvial dynamics and erosive processes. Likewise, IDW interpolation was applied to rainfall data from CELEC EP at the Guarumales camp to represent the spatial distribution of precipitation.

2.4 Phase IV: Zoning of unstable areas

Susceptibility analysis was generated by rasterization thematic cartography at a 0.5 m/pixel spatial resolution in a GIS environment. Homogeneous categories were defined based on the reclassification of value ranges, supported by bibliographic references and knowledge of the sector-specific variables, as summarized in Table 1. Zoning was obtained through map algebra within a GIS environment by applying a weighted overlay of the normalized raster layers. The selection of the criteria used is based on the methodology proposed by Mora and Vahrson [15], which defines five essential factors for evaluating landslide susceptibility: slope, lithology, soil moisture, seismic intensity, and rainfall intensity. Furthermore, the weighting of the factors was defined through a heuristic approach informed by the authors' technical judgment, supported by field observations and an understanding of the geomorphological and geological conditions of the study area. During the development of the susceptibility model, the relative importance of each variable was discussed and assigned considering both the local context and previous studies on landslide susceptibility mapping. In particular, the selection and weighting criteria were guided by methodological principles described in studies on heuristic susceptibility assessment, where the weights of conditioning factors are established through expert knowledge and interpretation of terrain conditions, as described by Reichenbach et al. [16]; which allowed the classification of susceptibility categories, resulting in the Eq. (1).

$$\begin{aligned}\text{Zoning} = {} & 0.15 \cdot L + 0.15 \cdot R + 0.20 \cdot S + 0.15 \cdot O \\ & + 0.10 \cdot C + 0.1 \cdot U + 0.05 \cdot D \\ & + 0.1 \cdot P\end{aligned} \quad (1)$$

where,

L: Lithology (dimensionless factor)
R: Electrical resistivity (Ω·m)
S: Slope (º)
O: Orientation (º)
C: Curvature (m-1)
U: Land use (dimensionless factor)
D: Distance to river (m)
P: Precipitation (mm)

A sensitivity analysis was conducted by varying the weights of the triggering and conditioning factors (slope and precipitation) by ±10% while keeping the total weight constant at 1. Similar variations have been commonly used in susceptibility modeling to evaluate the robustness of weighted overlay approaches [21]. For each scenario, a new susceptibility map was generated using the weighted overlay approach. The resulting maps were reclassified into seven

susceptibility subclasses. The percentage of the area occupied by each subclass was calculated from the number of pixels in each category. The sensitivity of the model was then evaluated by computing the variation in the percentage of area of each susceptibility subclass relative to the base scenario.

Table 1. Variables and weightings for the reclassification of unstable area zoning

Parameters and References	Susceptibility Classes				Weighting
	1 (Low)	2 (Moderate)	3 (High)	4 (Very high)	
(1) Lithology	Andesite	Schists (sericitic, chloritic and quartzose)	Graphitic schist, alluvial	Active colluvium, colluvial-alluvial	0.15
(2) Resistivity [9]	> 4000 Ω·m	2000–4000 Ω·m	75–2000 Ω·m	< 75 Ω·m Saturated zones	0.15
(3) Slope [22, 23]	0°–15°	16°–30°	31°–50°	> 50°	0.2
(4) Orientation [22, 24]	North (NW315º–NE45º)	South (SE135º–SW225º)	East (NE45º–SE135º)	West (SW225º–NW315º)	0.1
(5) Curvature [25, 26]	Negative values		Positive values		0.1
(6) Land use [22, 26]	Urban fabric	Dense forest	Shrubland	Water bodies	0.1
(7) Distance to river [26, 27]	> 150 m	50–100 m	25–50 m	< 25 m	0.05
(8) Precipitation [28, 29]	< 125 mm	125–250 mm	> 250 mm		0.15

3. RESULTS

3.1 Geoelectrical methods applied to unstable zones

A total of 16 ERTs and eight VESs were conducted throughout the Guarumales camp (Figure 3). Table 2 summarizes the technical parameters of geophysical surveys. Table 3 shows the resistivity ranges determined for the local measurements and correlated with the geotechnical boreholes previously.

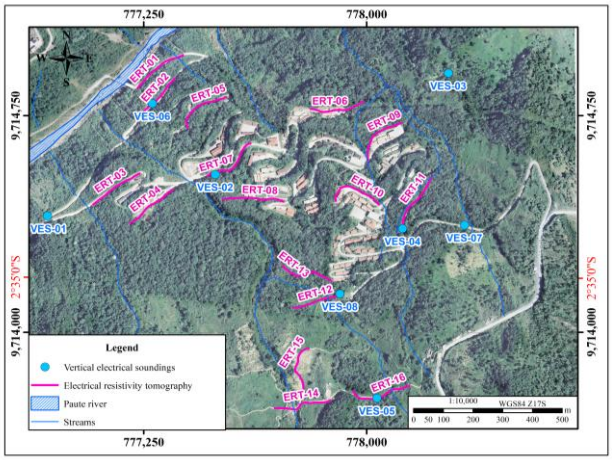

Figure 3. Location of the geophysical survey

In the southern sector of the camp, where ERT-12, ERT-13, ERT-14, ERT-15, and ERT-16 were carried out, horizons with resistivities below 200 Ω·m were observed, extending from the surface to approximately 10 m depth (Figure 4). At greater depths (> 30 m), low resistivities ranging from 400 to 1,000 Ω·m were identified, suggesting the presence of colluvial or residual soils, or highly weathered rock. VES-05 shows conductive intervals ranging from 4 to 100 m (Figure 5), with resistivities below 100 Ω·m, suggesting that the southwestern area at an elevation of 1,855 m is consistent with a water recharge environment. Resistivities below 150 Ω·m indicate the presence of saturated material, according to the classification presented in Table 3 of Alonso-Pandavenes et al. [9].

Table 2. Description of geoelectrical methods with the technical parameters used in the field survey

Number of Geophysical Surveys	Technical Parameters
15 ERTs	Length: 200 m, gradient array, electrode spacing: 5 m, approximate depth of investigation: 40 m
1 ERT	Length: 400 m, gradient array, electrode spacing: 5 m, approximate depth of investigation: 80 m
8 VESs	Length: 270 and 370 m, Schlumberger array, approximate depth of investigation: 147 m

Noe: ERT = Electrical Resistivity Tomography; VES = Vertical Electrical Soundings.

Table 3. Relationship between resistivity and lithological material

Lithology	Resistivity Range (Ω·m)
Saturated zones	< 75
Clayey material possibly saturated	75—175
Colluvial soil and residual soil, highly weathered and possibly saturated rock	175—1250
Colluvial	1,250—3,000
Weathered rock	3,000—7,000
Metavolcanic material / Igneous block	7,000—9,000
Fresh or massif rock	>9,000

In the intermediate slope area near the dining zone, at the camp elevation of 1,580 m, the geoelectric profiles ERT-06 to ERT-10 (Figure 3) show localized saturation zones down to

approximately 10 m depth. High resistivities are observed at the surface, associated with rock blocks within a colluvial matrix, while at depths where resistivities exceed 10,000 Ω·m, a continuous pattern along the survey suggests the presence of rock mass (Figure 4). ERT-16 indicates a possible fault zone between the bedrock massif and the colluvial deposit. ERT-07 shows high resistivity values (> 10,000 Ω·m) at a depth of approximately 10 m, corresponding to a massive rock block, although the layer is not laterally continuous. In contrast, ERT-02 does not exhibit a high-resistivity layer at depths of up to 40 m.

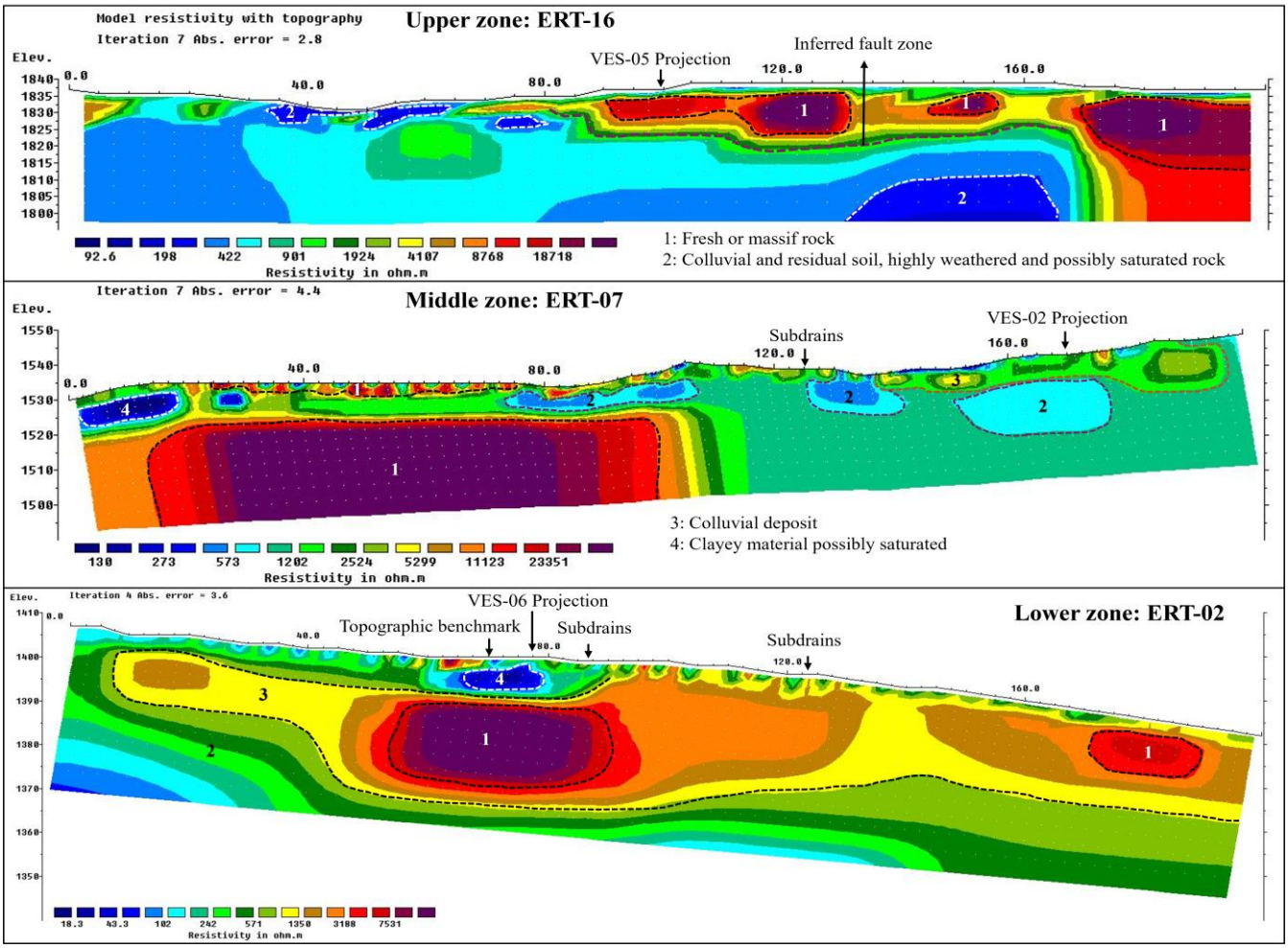

Figure 4. Campaign 2D ERT models for the upper, middle, and lower sectors of the study area, showing their correlation with VES surveys, subdrains, and topographic benchmarks installed as part of the macro-landslide monitoring system
Noe: ERT = Electrical Resistivity Tomography.

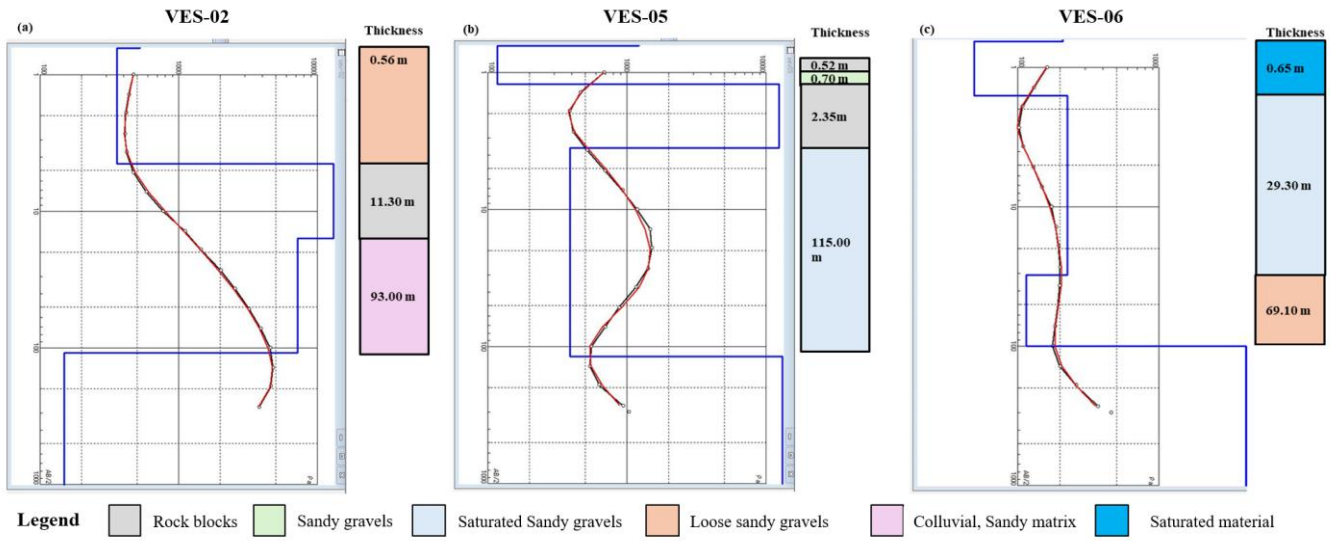

Figure 5. Representative VESs geoelectrical profiles
Noe: VES = Vertical Electrical Soundings.

Conversely, in the northern part of the camp, near the Paute River channel at the lower slope, the geoelectric profiles ERT-01, ERT-02, and ERT-05 (Figure 3) indicate saturation zones in fine-grained materials down to approximately 10 m, while VES-06 also shows saturation of these materials starting at 30 m depth (Figure 5). This suggests that the area functions as a groundwater discharge zone, consistent with its topographic position within the camp. Being at the lowest point, subsurface flow from upper areas tends to converge there, promoting moisture accumulation. Taken together, these geomorphological and hydrological conditions indicate that the observed saturations reflect the functioning of the local drainage system, where flow converges and discharges toward the base level. Table 3 summarizes the correlation between resistivity values and possible lithological types.

3.2 Application of Geographic Information System in analyzed variables

Based on the correlation between ERT and VES data with identified outcrops and historical boreholes, a basement composed of schists was determined at shallow depth in the northern part of the camp, whereas andesitic rocks are present at the surface in the eastern sector. Both lithological units are overlain by a thick colluvial deposit, according to historical boreholes and geoelectric profiles, which can reach up to 90 m in thickness in the southern part of the camp. Additionally, structural lineaments inferred from resistivity contrasts are delineated and may be associated with the basement, as shown in Figure 6.

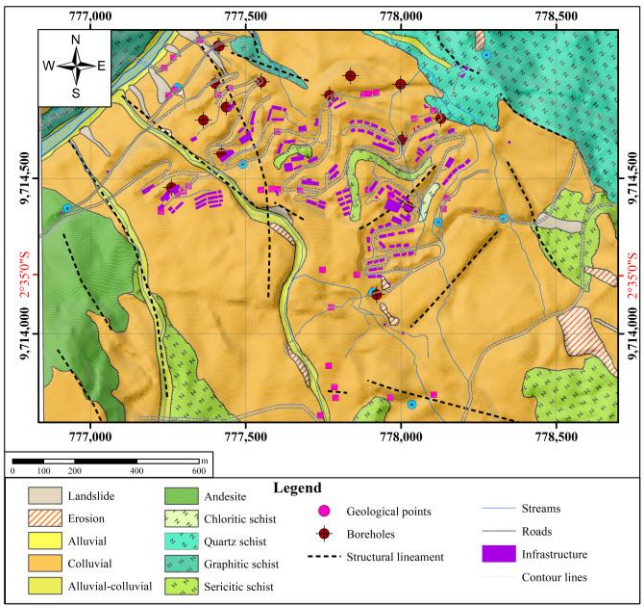

Figure 6. Lithological units and structural lineaments

The resistivities in the intermediate and lower slope areas range from 19 to 200 Ω·m; these values suggest water saturation and low-competence materials, which, based on the geoelectric profiles, are interpreted as near-surface saturations down to 10 m depth.

This could indicate the presence of springs or highly saturated zones, such as wet zones, consistent with site conditions. Conversely, historical geotechnical boreholes record more than 60 m of colluvial thickness in the lower slope area. In contrast, resistivity values approaching 10,000 Ω·m were obtained in the southern and western parts of the area, corresponding to fresh rock and large clasts, conditions that reduce the likelihood of instability in zones such as the intake point, treatment plant, and potable water reservoir located in the upper part of the camp (Figure 7).

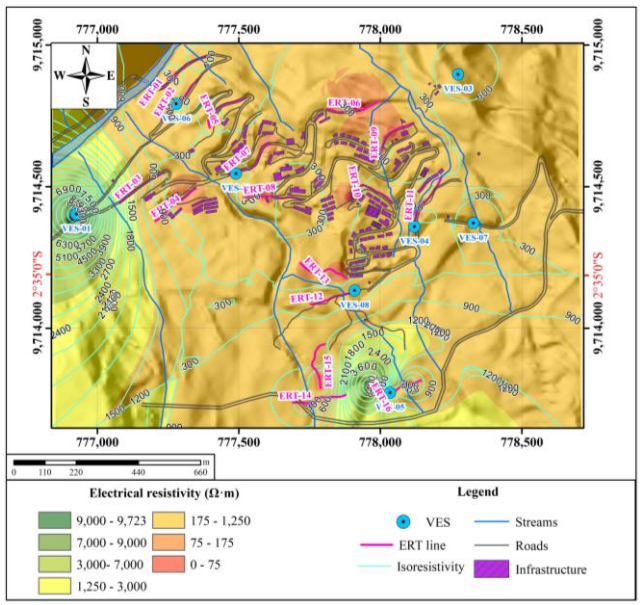

Figure 7. Surface distribution of its resistivity contours

The morphology of the area corresponds to a mountainous relief with pronounced topographic variations, featuring slopes exceeding 53° along drainage channels and steep hillslopes with gradients greater than 60° in interfluvial zones, as shown in Figure 8.

These morphologies, the drainage network, and poorly consolidated materials increase susceptibility to slope instability, with a higher incidence in the western and northwestern areas of the camp. In the study area, north-facing slopes dominate, with a smaller proportion facing south.

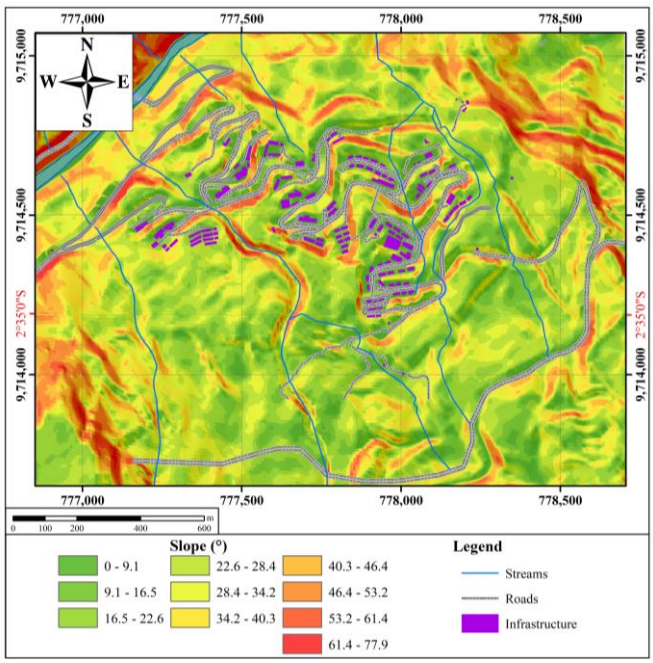

Figure 8. Representation of terrain slopes

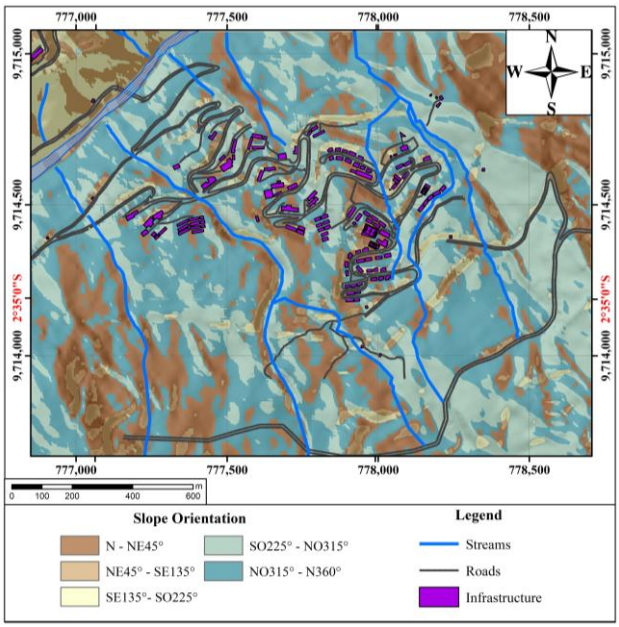

Figure 9. Orientation relative to geographic north

The alignment of the slopes in a similar direction to the overall slope gradient (toward the west) creates unfavorable conditions and increases the likelihood of instability processes (Figure 9).

The morphologies of the study area are characterized by concave curvatures, represented by negative values, associated with flow accumulation and promoting increased erosion and instability, and convex curvatures, represented by positive values, corresponding to ridges and watersheds, which exhibit greater stability, although with potential for local failures. Flat curvature zones, represented by values close to zero and predominant in the central sector, correspond to transition surfaces between concave and convex curvature, or vice versa, where instability depends on lithology and saturation degree (Figure 10). If the curvature transition zone is exceeded, subsidence or tension cracks may occur at these inflection points, serving as morphological indicators of instability zones.

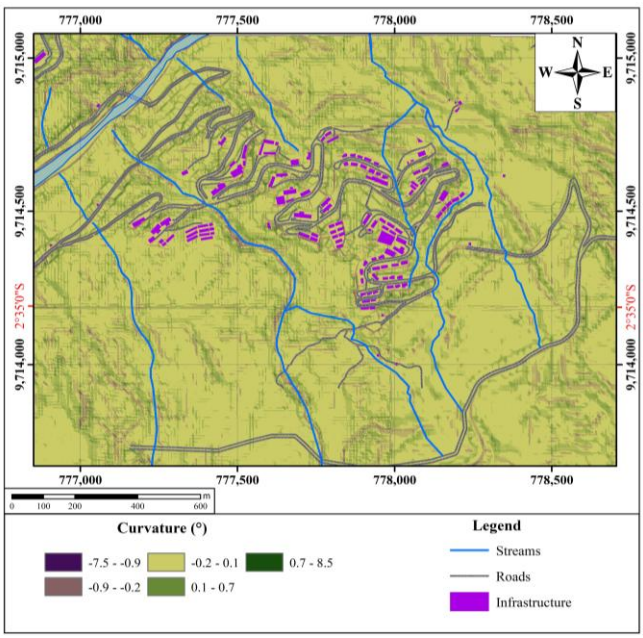

Figure 10. Representation of terrain curvature

In the study area, 64% is dense forest, mainly covering the western and eastern parts of the camp. Approximately 28% of the area is covered by shrubland, which, while contributing to erosion reduction, also promotes water accumulation and the formation of groundwater recharge zones, mainly in the southern part of the camp. Urban fabric and water bodies account for 7.8% and 0.2% of the area, respectively, and are susceptible to erosion processes, particularly on steep slopes (Figure 11).

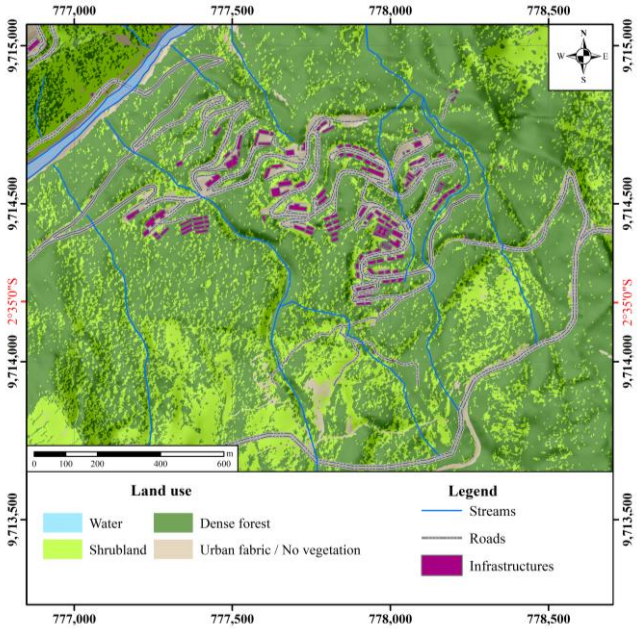

Figure 11. Representation of land use in the Guarumales camp

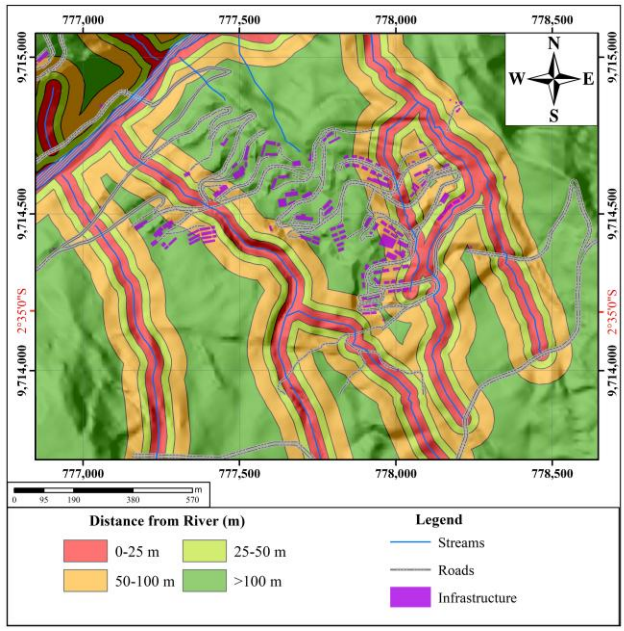

Figure 12. Distance ranges relative to the drainage network

Water bodies, rivers, and streams contribute to erosion and undercutting on slopes; areas within 0 to 25 m of drainage channels exhibit higher susceptibility to erosion (Figure 12) due to direct water flow and lateral undercutting. In this context, the eastern and western sectors of the camp could be affected by these natural phenomena. Although less intense, the influence of fluvial dynamics can extend up to 50 m from

the channel. Furthermore, areas located more than 50 m away show lower direct erosive impact from the drainage channels.

The study area experiences average monthly rainfall exceeding 250 mm/month (during the rainy season), which constitutes a critical factor for slope stability, as it intensifies water recharge in the upper slope, promotes saturation of poorly consolidated colluvial materials, and increases flow in the drainage network, enhancing erosion of slopes adjacent to the camp (Figure 13).

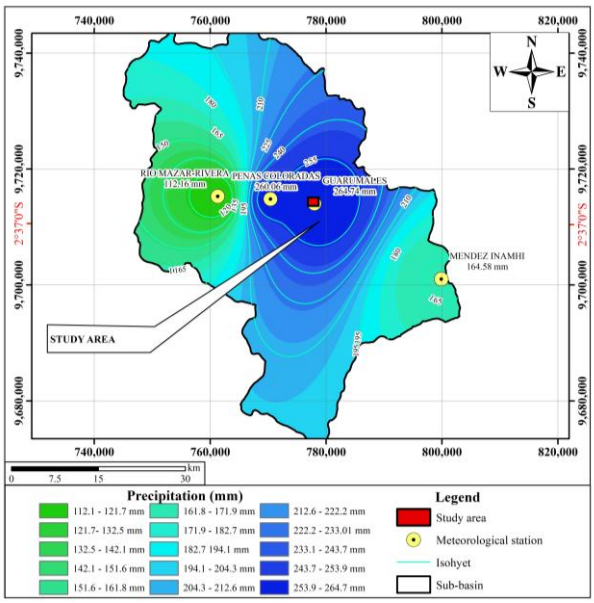

Figure 13. Isohyets and average monthly rainfall

3.3 Mapping of unstable zones

To improve the representation and interpretation of the susceptibility map, initially classified into four classes (Table 1), the index was reclassified into seven subclasses (Figure 14). The original classification led to excessive generalization, making it difficult to distinguish gradual variations. This process enabled more detailed zoning and visualization, thereby improving the interpretation and analysis of susceptibility. Based on the mapping of unstable zones (Figure 14), it was found that 7.87% of the area delineated as a macro-landslide by Robles [7], exhibits moderately high (7.53%) to high (0.34%) susceptibility to landslide, 20.42% of the area shows moderate susceptibility, and 65.06% of the area is classified as very low (25.88%) to low (39.18%). The estimated volume of the mass corresponding to the moderately high to high susceptibility zones is 915,936 m³, representing the sector with the greatest potential instability within the analyzed macro-landslide. This value was estimated considering the areas classified as moderate, moderately high, and high, and a depth of 15 m in zones characterized by low resistivity values.

The mapping (Figure 14) indicates higher susceptibility to mass movements along streams in the western and eastern parts of the camp, where erosion and lateral slope undercutting are evident. The occurrence of these processes coincides with areas closest to springs or drainage channels (<50 m; Figure 12), a condition classified as high to very high susceptibility (Table 1), putting infrastructure located within a 50-meter radius of the streams at risk.

Likewise, as shown in Figure 14, the sector located in the northwestern part of the camp, south of the Paute River, exhibits moderate to high susceptibility. This occurrence is directly correlated with material saturation and low consolidation of colluvial deposits, as analyzed using resistivity mapping (Figure 7), thereby putting the existing road infrastructure at risk.

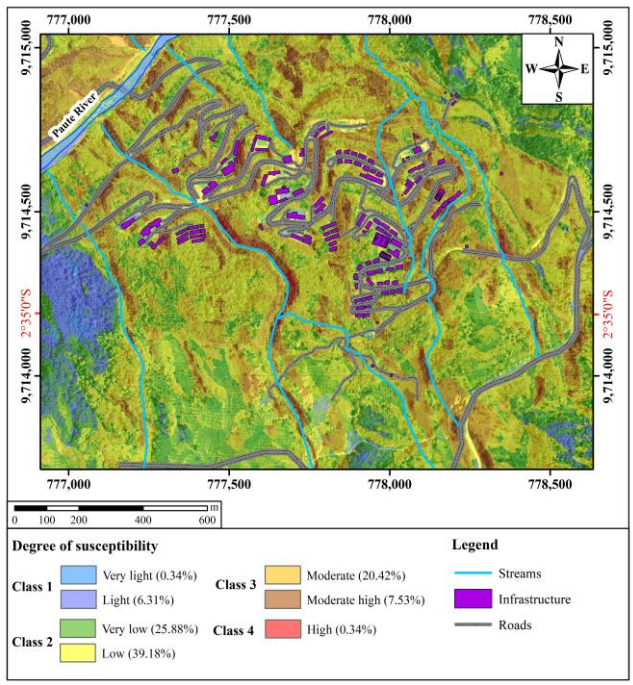

Figure 14. Mapping of unstable areas in the Guarumales camp

Table 4. Scenarios were evaluated for calculating the sensitivity index of the evaluated weights

Susceptibility Classes	Susceptibility Subclasses	Base (%)	Slope +10 Δ	Scenario Δ1	Slope -10 Δ	Scenario Δ2	Precipitation +10 Δ	Scenario Δ3	Precipitation -10 Δ	Scenario Δ4
Class 1	Very Light	0.34	0.34	0.00	0.96	0.62	0.35	0.01	0.34	0.00
	Light	6.31	6.23	-0.08	5.86	-0.45	6.23	-0.08	6.25	-0.06
Class 2	Very low	25.88	23.55	-2.34	24.56	-1.32	23.55	-2.34	25.67	-0.21
	Low	39.18	37.79	-1.39	38.58	-0.60	37.79	-1.39	37.90	-1.28
Class 3	Moderate	20.42	24.57	4.15	23.42	3.01	24.57	4.15	22.87	2.45
	Moderate high	7.53	7.15	-0.38	6.32	-1.22	7.15	-0.38	6.63	-0.91
Sensitivity index				1.20		1.04		1.20		0.70

The southeastern sector of the study area exhibits moderate to moderately high susceptibility, with mass movements associated with the low consolidation of colluvial deposits, compromising road infrastructure. The camp area exhibits moderate susceptibility, driven by sparse vegetation cover and steep slope gradients in the sector. Additionally, stream influence generates material saturation and erosion at the base of the slopes. The sector northwest of the Paute River exhibits

moderate instability. This occurrence is directly associated with abrupt morphologies; although no slope failures are currently evident, erosion processes that could affect this slope cannot be ruled out. In the 2012–2013 orthophotograph, erosion processes are observed in the upper part of the slope, composed of colluvial deposits.

Sensitivity analysis was performed by varying the weights of two key conditioning factors, slope and precipitation, by ±10%, while maintaining the total weight at 1. Four scenarios were evaluated (slope +10%, slope -10%, precipitation +10%, and precipitation -10%), yielding sensitivity indices of 1.20, 1.04, 1.20, and 0.70, respectively (Table 4). These low values indicate that the susceptibility model is relatively stable, robust, and not very sensitive to variations in the weighting scheme of the conditioning factors, as the overall susceptibility patterns remain largely consistent across the evaluated scenarios.

4. DISCUSSION

The landslide susceptibility map obtained in this study is based on the integration of multiple criteria: geophysical, geological, morphological, and hydrological.

Firstly, the interpretation of the geoelectric profiles revealed a strong correlation between low resistivity (<75 Ω·m) and the presence of saturated, low competence colluvial materials. This finding is consistent with the observations of Urgilez Vinueza et al. [4], who associated these values with areas of high landslide susceptibility in the PIHC. However, it is important to consider that spatial variation in ERT resistivities can be influenced by heterogeneity in the deposits, introducing uncertainties in the precise delineation of layers.

Regarding the weights assigned in the multi-criteria weighting, although these are based on heuristic approaches validated in the scientific literature [14], their application involves a certain degree of subjectivity.

From a hydrological perspective, a clear relationship was identified between proximity to drainage channels (< 50 m), steep slopes (> 53°), and low resistivity values, suggesting a synergy between saturation, surface runoff, and fluvial erosion, as reported by Macías et al. [30]. However, the spatial interpolation of precipitation may introduce uncertainty due to the low density of meteorological stations in mountainous areas such as Guarumales. Increasing the number of stations or integrating regional climate models would allow a more accurate representation of the rainfall regime, improving the estimation of triggering factors for instability.

From a geomorphological perspective, concave curvatures and steep slopes favor moisture accumulation, creating conditions conducive to instability. However, the current model does not incorporate temporal variations of the water table, which represents a limitation, particularly during extreme rainfall events—those exceeding the 95th–99th percentile or exhibiting high intensities over short periods—capable of rapidly saturating the terrain, as observed in analyses of extreme rainfall events in the southern Andes of Ecuador [31]. Previous studies, such as Alonso-Pandavenes et al. [9] highlight the importance of integrating transient groundwater flow analyses to understand the dynamic evolution of these processes.

Although the susceptibility mapping (Figure 14) shows spatial coherence with the observed field processes and constitutes a relevant technical tool for risk management, it is important to consider that susceptibility levels may vary over short time periods. For example, areas classified as moderately susceptible, such as the northeastern sector of the camp, could experience significant instability during seasonal saturation events or anthropogenic activities (construction or deforestation). Conversely, areas categorized as stable (very low to low susceptibility), such as most of the residential, casino, and dining areas, could degrade due to changes in land use. Therefore, the mapping should be interpreted as a dynamic input, that can be updated. These factors reinforce the need to maintain a permanent monitoring system, such as the one currently implemented by CELEC EP [5], which should focus on sectors designated as moderately high and high in susceptibility to refine evaluations and continuously update the mapping. To evaluate the consistency of the results obtained in the susceptibility mapping, the resistivity profile A–A' (Figure 15) was generated, crossing the northern sector of the camp from the upper slope in the east to the lower slope in the west. This profile allows analysis of the relationship between the resistivity distribution, geomorphological conditions, and the susceptibility levels identified in the mapping.

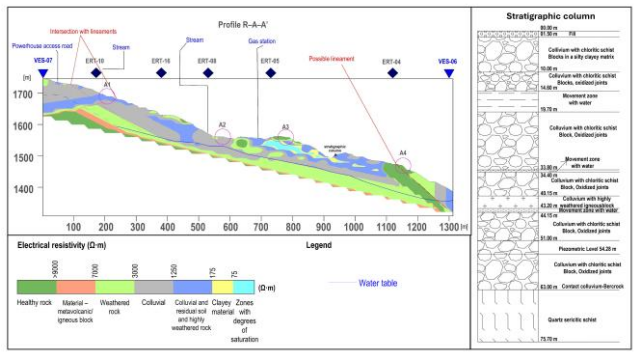

Figure 15. Section A-A' crossing the northern sector of the camp from the upper slope in the east to the lower slope in the west

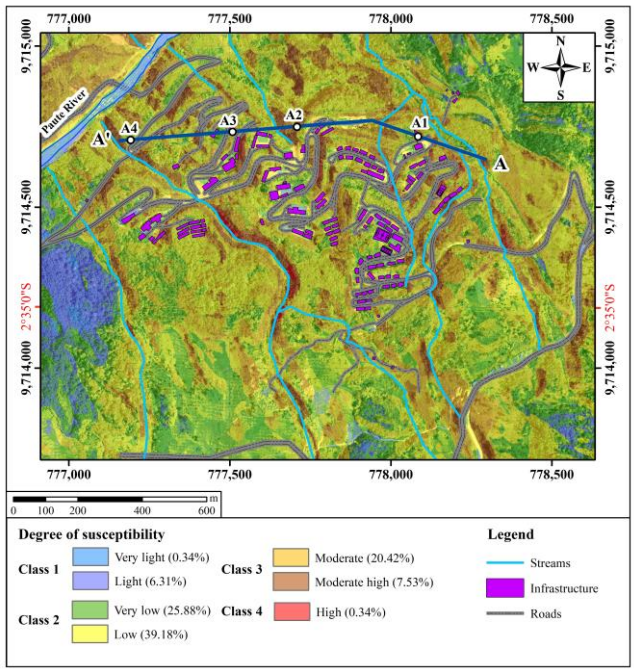

Figure 16. Section location in plan view

Four points of interest are identified along with this profile,

as shown in Figure 16. At point A1, located in the northeastern sector of the camp and corresponding to the beginning of the profile, residual strata and weathered rock outcrop at the surface, followed by a layer of colluvial material. With increasing depth, resistivity values increase, reflecting the transition from weathered rock to igneous rock, and, finally, to fresh rock. This behavior is consistent with the moderate susceptibility level determined for the sector, attributable to the superficial presence of colluvial and residual materials, which exhibit a high propensity for landslide under steep-slope conditions.

Point A2, located approximately 600 m from the beginning of profile A–A', is characterized by the presence of thick colluvial deposits overlying a layer of weathered rock. Compared to the susceptibility map, this sector corresponds to an area with low to moderate susceptibility. Despite intermediate resistivity values, instability is limited by gentle slopes and the progressively decreasing influence of fluvial processes with increasing distance from the stream.

Point A3, located approximately 800 m from the beginning of the profile, exhibits at the surface a layer of weathered rock interbedded with colluvial material. At greater depth, a marked decrease in resistivity values is observed, interpreted as the presence of highly saturated materials, possibly saturated clays, underlying thick colluvial deposits and weathered rock. According to the susceptibility mapping, this sector is classified as moderately high to high susceptibility. This configuration is conducive to instability, as competent layers are identified at both the upper and lower levels. At the same time, the intermediate zone is dominated by lower-strength strata with high saturation, which could constitute a preferential sliding surface.

Finally, point A4, located approximately 1,200 m from the beginning of profile A–A' in the northwestern sector of the camp, is characterized by highly competent layers of fresh rock overlain by weathered rock. This stratigraphic condition is consistent with the susceptibility mapping, which classifies the sector as low to very low susceptibility, in accordance with the high resistivity values and the relatively gentle slopes.

In general, the spatial correspondence between the mapping of unstable areas and the geoelectric profile A–A' shows a high internal consistency, supporting the applicability and robustness of the proposed methodology for similar studies in complex geological settings.

Finally, this multidisciplinary approach enabled a coherent representation of terrain conditions and their relative stability. However, the results also reveal limitations that need to be addressed to strengthen the method's scientific robustness of the method. The heterogeneity of colluvial deposits introduces uncertainty in delineating resistivities, underscoring the need to increase the density of ERT–VES profiles to better define transitional zones. Furthermore, the multi-criteria weighting used, although supported by specialized literature, retains a subjective component that could be refined using multivariate statistical methods or machine learning models to quantify each variable's actual weight. Similarly, the absence of direct geotechnical information (such as triaxial tests, permeability, unit weights, undrained and drained shear strength parameters) limits the validation of geoelectric interpretations. Incorporating these parameters would allow for a more precise correlation between resistivity ranges and the material's effective competence. Finally, future studies should integrate transient hydrogeological monitoring (water table levels and pore pressures) to capture the effects of extreme events, thereby strengthening the conceptual framework underpinning this scientific and technical contribution. A total of 915,936 m³ is classified as areas of moderately high to high susceptibility to landslides.

5. CONCLUSIONS

The integration of geological, geomorphological, hydro-meteorological, and geoelectric information enabled precise characterization of the physical conditions controlling instability at the Guarumales camp. This is due to the combination of fractured schists, thick colluvial deposits, and high moisture levels, which create an environment highly susceptible to mass movements. Steep slopes (>53°), concave curvatures, proximity to drainage channels (<25 m), and rainfall exceeding 250 mm/month (seasonal rainy period, three months) are key conditioning and triggering factors, that intensify saturation and the loss of material strength.

During this research, electrical resistivity proved to be a critical parameter for discriminating between saturation domains and material competence. Resistivity values below 75 Ω·m were associated with fragile, saturated materials, while values above 7,000 Ω·m indicated more competent, stable conditions.

The correlation between ERT and VES methods, together with geomorphological factors, enabled the generation of a spatial map of landslide susceptibility, clearly identifying areas of highest priority for risk management. The areas of greatest interest are those classified as high, moderately high, and moderate susceptibility, accounting for 0.34%, 7.53%, and 20.42% of the area delineated as the macro-landslide zone, respectively. This study provides a methodological baseline for stability assessment in complex, mountainous terrain with similar characteristics, using combined geophysical methods.

The susceptibility mapping shows that high-susceptibility areas are concentrated along drainage channels and their margins, forming critical corridors that increase exposure of roads and infrastructure points. Although most buildings are in low-susceptibility zones, the influence of high-susceptibility strips highlights the need for continuous preventive management.

In terms of risk management and mitigation, the results of this study provide a technical input for mapping sectors that require optimization and reinforcement, and for identifying areas where erosion control and drainage improvements would be most effective, such as the north-northwestern sector of the camp, which exhibits the highest susceptibility. Additionally, the saturated domains identified through geoelectric surveys facilitate the design of engineering solutions, such as deep horizontal drains, lined channels, slope reconfiguration, or revegetation on low-competence slopes.

The results show strong agreement between the susceptibility mapping, geoelectric profiles, and the geomorphological conditions observed in the field, with spatial correspondence between low-resistivity domains, steep slopes, and proximity to drainage channels reinforcing the internal consistency of the analysis and the interpretation of the conditioning factors of instability. This supports the robustness of the adopted methodological approach and the reliability of the mapping as a tool for risk assessment and management in the Guarumales camp. To strengthen this methodological contribution and expand its applicability, future research should incorporate geotechnical parameters that allow quantitative correlation of resistivity ranges with the mechanical properties of soil and rock, to validate and

calibrate the identified geoelectric domains, as well as integrate seasonal monitoring (rainy and dry periods) of the water table. In this regard, the study provides a solid technical and scientific framework for assessing unstable slopes and reducing of risk in critical infrastructure, establishing methodological bases that can be replicated in other large-scale projects in mountainous areas of Ecuador and the Andean region.

ACKNOWLEDGMENT

To the Master in Geotechnics (FICT-ESPOL) for all the knowledge imparted and academic excellence. The CIPAT-ESPOL provides logistical support, personnel, and geophysical equipment for field research. This work was supported by the research project "Applied Research Program in Geological and Geotechnical Studies for Hydropower Plant Monitoring at the CELEC SUR Business Unit", Code CIPAT-CIPAT-001-2023 of the ESPOL Polytechnic University.

REFERENCES

[1] Pourghasemi, H.R., Pouyan, S., Bordbar, M., Golkar, F., Clague, J.J. (2023). Flood, landslides, forest fire, and earthquake susceptibility maps using machine learning techniques and their combination. Natural Hazards, 116(3): 3797-3816. https://doi.org/10.1007/s11069-023-05836-y

[2] Caleca, F., Lombardo, L., Steger, S., Tanyas, H., Raspini, F., Dahal, A., Tofani, V. (2025). Pan-European landslide risk assessment: From theory to practice. Reviews of Geophysics, 63(1): e2023RG000825. https://doi.org/10.1029/2023RG000825

[3] Regmi, S., Dahal, R.K. (2024). Consequences of slope instability and existing practices of mitigation in hydropower projects of Nepal. Geoenvironmental Disasters, 11(1): 26. https://doi.org/10.1186/s40677-024-00289-2

[4] Urgilez Vinueza, A., Robles, J., Bakker, M., Guzman, P., Bogaard, T. (2020). Characterization and hydrological analysis of the guarumales deep-seated landslide in the tropical ecuadorian andes. Geosciences, 10(7): 267. https://doi.org/10.3390/geosciences10070267

[5] CELEC EP. CELEC SUR – Corporación Eléctrica del Ecuador (Electricity Corporation of Ecuador). https://www.celec.gob.ec/celecsur/, accessed on Mar. 20, 2026.

[6] Agencia de Regulación y Control de Electricidad. (2025). Panorama Eléctrico. https://arconel.gob.ec/wp-content/uploads/downloads/2025/05/Revista28-versionGobierno-v5.pdf.

[7] Robles, J. (2020). Caracterización y microzonificación del Macro deslizamiento Guarumales y propuesta de medidas de mitigación, Azuay-Ecuador.

[8] Universo, E. (2020). Aluvión bloquea el paso entre Azuay y Morona Santiago. Https://Www.Eluniverso.Com/Noticias/2020/06/02/Nota/7859286/Deslizamiento-Amaluza-Sevilla-Oro-Azuay/.

[9] Alonso-Pandavenes, O., Torrijo, F.J., Garzón-Roca, J., Gracia, A. (2023). Early investigation of a landslide sliding surface by HVSR and VES geophysical techniques combined, a case study in Guarumales (Ecuador). Applied Sciences (Switzerland), 13(2): 1023. https://doi.org/10.3390/app13021023

[10] Solórzano, J., Morante-Carballo, F., Montalván-Burbano, N., Briones-Bitar, J., Carrión-Mero, P. (2022). A systematic review of the relationship between geotechnics and disasters. Sustainability, 14(19): 12835. https://doi.org/10.3390/su141912835

[11] Das, S., Kanungo, D.P. (2023). A critical review on landslide susceptibility zonation: Recent trends, techniques, and practices in Indian Himalaya. Natural Hazards, 115(1): 23-72. https://doi.org/10.1007/s11069-022-05554-x

[12] Bravo-López, E., Castillo, T.F. Del, Sellers, C., Delgado-García, J. (2023). Analysis of conditioning factors in Cuenca, Ecuador, for landslide susceptibility maps generation employing machine learning methods. Land, 12(6): 1135. https://doi.org/10.3390/land12061135

[13] Carrión-Mero, P., Solórzano, J., Malavé-Hernández, J., Martínez-Angulo, J., Javier, M.F., Morante-Carballo, F. (2024). Mapping groundwater potential zones for sustainable agricultural development in Entre Ríos, Ecuador. International Journal of Design & Nature and Ecodynamics, 19(3): 817-830. https://doi.org/10.18280/ijdne.190312

[14] Torrijo, F.J., Álvarez, S., Garzón-Roca, J. (2024). A case study of a macro-landslide in the high mountain areas of the Ecuadorian Andes: “La Cría” at the Azuay Province (Ecuador). Land, 13(12): 2047. https://doi.org/10.3390/land13122047

[15] Mora, S., Vahrson, W.G. (1994). Macrozonation methodology for landslide hazard determination. Bulletin of the Association of Engineering Geologists, 31(1): 49-58. https://doi.org/10.2113/gseegeosci.xxxi.1.49

[16] Reichenbach, P., Rossi, M., Malamud, B.D., Mihir, M., Guzzetti, F. (2018). A review of statistically-based landslide susceptibility models. Earth-Science Reviews, 180: 60-91. https://doi.org/10.1016/j.earscirev.2018.03.001

[17] El Makrini, S., Boualoul, M., Mamouch, Y., El Makrini, H., Allaoui, A., Randazzo, G., Roubil, A., El Hafyani, M., Lanza, S., Muzirafuti, A. (2022). Vertical electrical sounding (VES) technique to map potential aquifers of the Guigou plain (Middle Atlas, Morocco): Hydrogeological implications. Applied Sciences, 12(24): 12829. https://doi.org/10.3390/app122412829

[18] Florinsky, I. (2025). Digital Terrain Analysis. Elsevier.

[19] Pronk, M., Hooijer, A., Eilander, D., Haag, A., et al. (2024). DeltaDTM: A global coastal digital terrain model. Scientific Data, 11(1): 273. https://doi.org/10.1038/s41597-024-03091-9

[20] Sharma Banjade, S., Rai, N., Subedi, B. (2023). Comparison of supervised classification algorithms using a hyperspectral image for land use/land cover classification. Environmental Sciences Proceedings, 29(1): 59. https://doi.org/10.3390/environmentsci29100059

[21] Chalkias, C., Ferentinou, M., Polykretis, C. (2014). GIS supported landslide susceptibility modeling at regional scale: An expert-based fuzzy weighting method. ISPRS International Journal of Geo-Information, 3(2): 523-539. https://doi.org/10.3390/ijgi3020523

[22] Mafigiri, A., Khanan, M.F.A., Abdullah, R.A. (2025). A review of GIS-based landslide susceptibility and hazard modeling considering the influence of topographic

parameters on rainfall spatial variability. Modeling Earth Systems and Environment, 11(6): 427. https://doi.org/10.1007/s40808-025-02615-5

[23] Foumelis, M., Lekkas, E., Parcharidis, I. (2018). Landslide susceptibility mapping by GIS-based qualitative weighting procedure in Corinth area. Bulletin of the Geological Society of Greece, 36(2): 904. https://doi.org/10.12681/bgsg.16840

[24] Ashraf Mohammed, O., Kamal Hamaamin, H., Azad, J., Rasooli, S., Li, H. (2025). Spatial prediction of landslide susceptibility using the data-mining algorithm (case study: Kamyaran county). Frontiers in Earth Science, 13: 1619876. https://doi.org/10.3389/feart.2025.1619876

[25] Xu, K., Zhao, Z., Chen, W., Ma, J., Liu, F., Zhang, Y., Ren, Z. (2024). Comparative study on landslide susceptibility mapping based on different ratios of training samples and testing samples by using RF and FR-RF models. Natural Hazards Research, 4(1): 62-74. https://doi.org/10.1016/j.nhres.2023.07.004

[26] Ou, L., Huang, C., Cao, Y. (2024). Research on landslide hazard assessment based on improved analytic hierarchy process optimizing multiple rainfall indicators. Discover Applied Sciences, 6(8): 409. https://doi.org/10.1007/s42452-024-06119-2

[27] Duan, Y., Zhang, X., Zhao, W., Han, X., Lv, L., Yao, Y., Wang, Q. (2024). A study of landslide susceptibility assessment and trend prediction using a rule-based discrete grid model. Remote Sensing, 16(24): 4740. https://doi.org/10.3390/rs16244740

[28] Leta, E.D., Diriba, D., Abrha, N., Karuppannan, S. (2025). Landslide susceptibility mapping using geospatial technology in the case of the Gidabo watershed, Main Ethiopian Rift. Scientific African, 29: e02928. https://doi.org/10.1016/j.sciaf.2025.e02928

[29] Peiro, Y., Volpe, E., Ciabatta, L., Cattoni, E. (2024). High resolution precipitation and soil moisture data integration for landslide susceptibility mapping. Geosciences, 14(12): 330. https://doi.org/10.3390/geosciences14120330

[30] Macías, L., Quiñonez-Macías, M., Toulkeridis, T., Pastor, J.L. (2024). Characterization and geophysical evaluation of the recent 2023 Alausí landslide in the northern Andes of Ecuador. Landslides, 21(3): 529-540. https://doi.org/10.1007/s10346-023-02185-6

[31] Urgilés, G., Célleri, R., Bendix, J., Orellana-Alvear, J. (2024). Identification of spatio-temporal patterns in extreme rainfall events in the Tropical Andes: A clustering analysis approach. Meteorological Applications, 31(5): e70005. https://doi.org/10.1002/met.70005